Theoretical and numerical investigation of the mode I delamination of composite laminate with uneven thickness

Pan Xiao[1], Jiang Yi[1]*, Li Mingjun[1]

[1] School of Aerospace Engineering, Beijing Institute of Technology, Beijing, 100081, China

Abstract

In this paper, a theoretical analysis model and two simulation methods are applied to characterize the quasi-static and fatigue delamination of composite laminate with uneven thicknesses. The test data of partially reinforced double-cantilever beam (DCB) were used as benchmark to verify the analysis model and simulation, and cohesive zone models (CZMs) and virtual crack closure technique (VCCT) are used in simulation. It's shown that the partially reinforced DCB has a unique double-peak load-displacement relationship, and produces instability development during the delamination. By comparing the results of simulation and experiment, it is found that the simulation based on the exponential CZM can simulate the delamination process of partially reinforced DCB under both quasi-static and fatigue loading; while VCCT method will generate a straight delamination front edge in the area of reinforcement, and lost the micro-damage of the previous loading step between load steps, and result in an incorrect delamination behavior.

Keywords: Delamination; cohesive zone model; virtual crack closure technique; finite element method

Nomenclature

a	Delamination length
a_0	Initial crack length
a_1	Longitudinal distance between the front of reinforced area and the loading point
A_0	Initial loading area
A_D	Micro-failure loading area
C_f	Critical damage loading ratio
CZM	Cohesive zone model

*Corresponding author. give full affiliation and *E-mail address:* jy2818@163.com

$\mathrm{d}a/\mathrm{d}N$	Growth rate of a crack
D, $\dot{D}$	Damage variable and its derivative
D_c, $\dot{D}_c$	Damage variable caused by cyclic loading and its derivative
DCB	Double-cantilever beam
D_m, $\dot{D}_m$	Damage variable caused by monotonic loading and its derivative
e	Natural constant
E, G, μ	Young's modulus, shear modulus and Poisson's ratio of the material
$F_{ii'}$, $F_{jj'}$,	Vertical internal force on node i and j
G	Energy release rate
G_I	Energy release rate of mode I
G_{Ic}	Critical energy release rate if mode I
h_i,w_i	Height and width of part i
$H(\cdots)$	Heaviside function
I_i	Second moment of inertia in part i
k_n	Loading/unloading stiffness in element
l	Length of the beam
LEFM	Liner-elastic fracture mechanics
M	Applied moment of the beam
P	Loading force in vertical direction on the upper arm of the specimen
q	Mode–mixity ratio
R	Load ratio
T_n, T_t	Normal and shear cohesive tractions
$\bar{T}$	Resultant traction
T_{CZ}	Cohesive traction
u	Opening distance of the specimen
UEL	A user-defined subroutine
U_s	Strain energy of the specimen
VCCT	Virtual crack closure technique
X_1, X_2	Length and width coordinates of the delamination
α	Contact penalty coefficient
δ_0	Cohesive length
δ_f	Initial undamaged cohesive normal strength
δ_Σ	Accumulated cohesive length
Δa, w	Element length and width
Δu	Separation
Δu_n, Δu_t	Normal and shear separation
$\Delta\bar{u}$, $\Delta\dot{\bar{u}}$	Resultant separation and its derivative
σ_{max}	Maximum stress that damaged surface can withstand
$\sigma_{max,0}$	Initial cohesive strengths under monotonic loading

1 Introduction

Composite laminates are widely used in modern architecture and mechanical structure due to their light weight and impressive strength[1]. In the past several years, a large number of key mechanical components have been replaced by composites and adhesive joints, therefore the delamination of composite laminate, which is one of the main forms of composite failure, has also received more attention[2–4].

Liner-elastic fracture mechanics (LEFM)[5,6] and cohesive zone models (CZMs)[7,8] are the two crucial theories for the delamination failure of composite laminate. The virtual crack closure technique (VCCT) and the Paris' law[9] are derived under LEFM, and have already become well-established methods in computing the energy release rate G and predicting fatigue crack growth for a long time[10]. Meanwhile, cohesive zone models (CZM) have also been a successful tool for accurately modeling delamination and are equally popular in the research community as in the industry [11,12]. It's distinguished from LEFM-based models by building the relationship between traction and separation near the crack tip [13,14], and using a damage variable D to define the damage on both monotonic loading and cyclic loading[15].

Nowadays, many studies on delamination of composite laminate have been made, mainly focus on the analysis of delamination failure process on double-cantilever beam (DCB) specimen [16,17]. Mall S. et al.[18] carried out a study to compare the experimental and analytical results of an adhesively bonded composite joint, and characterized both the static and fatigue mechanism under mode I and mixed I and II mode loadings. Spandan M. et al.[19] proposed a bi-linear cohesive failure model to simulate fatigue crack propagation in polymeric materials, and a finite element calculation based on the model was built to prove its accuracy. Roe K.L. et al.[15] studied a new model of cohesive failure under fatigue loading. Instead of using bi-linear cohesive failure law and Paris equation, a different model based on exponential cohesive zone law of Xu and Needleman[20] and irreversible constitutive equation for the cyclic interface traction–separation behavior was proposed. Turon A. et al.[21] conducted a method of determining constitutive parameters for the simulation of progressive delamination, by considering the size of the cohesive finite element, the length of the cohesive zone, and the minimum penalty stiffness necessary for the constitutive equation.

Bi-linear cohesive failure model and exponential cohesive failure model are the two most used model for cohesive failure calculation. Due to the concise characteristics, bi-linear model has been widely used on both monotonic loading[22–24] and cyclic loading[25,26] on two or three-dimensional analysis, and embedded in some finite element programs and softwares. At the same time, the exponential cohesive model, which can be expressed by a single expression and a continuous curve, is closer to the constitutive of the material, and therefore shows more accuracy than the bi-linear cohesive model. Fan J. et al.[27] established a subroutine based on two-dimensional exponential cohesive model and fatigue damage accumulative criterion in the finite element software, which was found in good accordance with the existing experimental results. Busto S. et al.[28] considered a user defined two-dimensional element subroutine with general implementation of cohesive zone models, which enables not only the modeling of crack initiation and growth under both monotonic and cyclic loading conditions, but also the calculation in conjunction with other damage development criteria.

The VCCT method has also been widely used [29–31], due to its simpler structure, fewer input param-

eters, and was incorporated into many commercial finite element software earlier. Pirondi A. et al.[32] presented a comparison between the bi-linear CZM and VCCT for three-dimensional fatigue debonding, found the two models are in overall good agreement with each other on DCB and end loaded split (ELS) geometry. Heidari R.M. et al.[33] conducted another comparison of VCCT, CZM and extended finite element method (XFEM) in unidirectional DCB composite samples. The results show that VCCT does not have ability to accurately model delamination propagation in multilayered DCB composites, and is very mesh sensitive at the same time. But VCCT is a simple and effective way to predict the delamination initiation. VCCT and CZM show advantages in different aspects, therefore in recent years, more and more researches are more inclined to use the method of combining both the models [34–36].

The above studies are based on the delamination failure calculation of DCB, ELS or other similar simple standard tests, with composite materials in layered structures and uniform thickness, There are not many studies on the delamination process of non-uniform materials. Carreras L. et al.[37] provided a benchmark test for validating 3D simulation methods for delamination growth under quasi-static and fatigue loading, with a comprehensive benchmark case consisting of a DCB-like specimen and partially reinforced arms.

This work will be combined with the benchmark test of Carreras, and study the delamination growth of partially reinforced DCB under static and fatigue loads. The research will combine the models of VCCT and CZM to compare the effects of different delamination simulation methods on the results of delamination calculations. At the same time, combined with the analysis model, the delamination mechanism under different conditions is calculated. The research mainly takes the load-displacement curve of the specimen and the position and shape of the delamination front as the observation object, which will provide reference for subsequent researchs and simulations.

2 VCCT and exponential cohesive failure models

2.1 VCCT

VCCT is a well-known technique based on LEFM, which calculates the evaluation of the energy release rate G and mode–mixity ratio q for cracks in homogeneous materials [32]. VCCT is based on the assumption that the strain energy released when a crack is extended by a certain amount is the same as the energy required to close the crack by the same amount, and the stress state at the crack tip is steady during the crack propagation. The assumption is acceptable if the propagation length being small compared with the crack length [38].

A schematic of elements along the crack tip is illustrated in Figure 1, that the node where the crack tip located at the beginning is i, and the vertical internal force on node i is $F_{ii'} = F_0$. When the damage continues to develop, the force $F_{ii'}$ decreases linearly to 0, the crack tip advances to node j and $F_{jj'} = F_0$, while node i split into nodes i and i', with the distance v_i at between. Base on the assumption of VCCT model, the mode I energy release rate G_I is:

$$G_I = \frac{v_i F_0}{2w\Delta a}$$

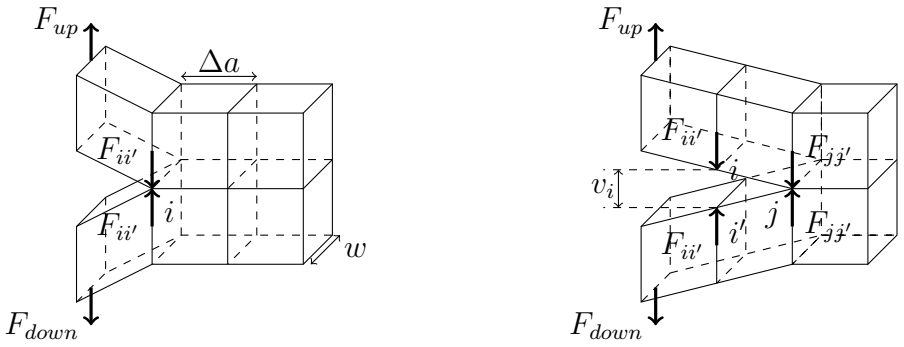

Figure 1: Schematic of mesh debonding in VCCT model

with Δa is the element length and w is the element width. Nodes i and i' will start to release when $f = \frac{G_I}{G_{Ic}} \geq 0$, G_{Ic} is the critical Mode I energy release rate.

2.2 Cohesive Zone Model (CZM)

CZM uses cohesive finite elements to model material discontinuities. A CZM based on Needleman [39] provides exponential cohesive failure relationship between the cohesive traction T_{CZ}, and the material separation Δu. Given the normal and shear separation as Δu_n, Δu_t, and normal and shear cohesive tractions as T_n, T_t, the relationship between them under monotonic loading can be expressed as:

$$T_n = \sigma_{max,0} \exp\left(1.0 - \frac{\Delta u_n}{\delta_0}\right) \left\{ \frac{\Delta u_n}{\delta_0} \exp\left(-\frac{\Delta u_t^2}{\delta_0^2}\right) + (1.0 - q)\frac{\Delta u_n}{\delta_0}\left[1.0 - \exp\left(-\frac{\Delta u_t^2}{\delta_0^2}\right)\right]\right\} \tag{1a}$$

$$T_t = 2\sigma_{max,0} q \frac{\Delta u_t}{\delta_0}\left(1.0 + \frac{\Delta u_n}{\delta_0}\right) \exp\left(1.0 - \frac{\Delta u_n}{\delta_0} - \frac{\Delta u_t^2}{\delta_0^2}\right) \tag{1b}$$

In which, $\sigma_{max,0}$ is the initial cohesive strengths under monotonic loading, i.e., the maximum normal traction a cohesive element can reach; δ_0 is the cohesive length, i.e., the normal separation required to reach the cohesive strength in normal loading. The critical normal energy release rate G_{Ic} can be defined as the area below the curve in Figure 2. The parameter q is the ratio between shear and normal energy release rate, representing the percentage of separation affected by shear. In pure normal monotonic loading, $q = 0$, $T_t = 0$,

$$T_n = \sigma_{max,0} \times e^{(1-\frac{\Delta u_n}{\delta_0})} \times \frac{\Delta u_n}{\delta_0}$$

Considering the occurrence of micro-failure on the contact surface, a micro-failure with area A_D appears on the surface with initial area A_0. In order to establish a fatigue failure model, it is necessary to introduce a damage variable D that is independent of stress and deformation. D is a state variable representing the density of micro-fracture on the contact surface, $D = (A_D/A_0)$. According to the definition of D, it can also represent the ratio of the maximum stress σ_{max} that a micro-failed surface can withstand, and the maximum stress $\sigma_{max,0}$ that can be withstood without damage, which is $\sigma_{max} = \sigma_{max,0}(1 - D)$. Since the failure parameters are independent of stress and deformation, but the accumulation of stress and deformation caused the development of failure parameters, it's reasonable to assume that there is $\dot{D} = \dot{D}(T, \Delta u, D)$ with following properties:

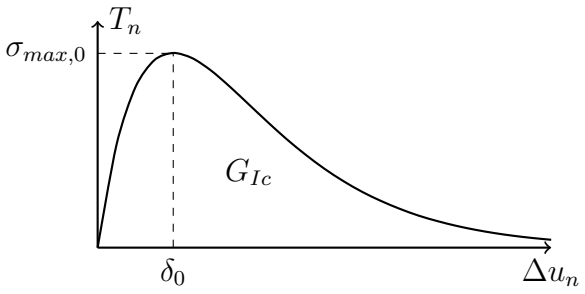

Figure 2: The traction-separation relationship in pure normal loading

1. The damage starts to accumulate only when the deformation or cumulative deformation exceeds a critical value;

2. The increase in damage is related to the increase in deformation, and the weight is determined by the average of the loading;

3. There is a load limit value: when the load is lower than this value, the material can circulate indefinitely without damage.

Therefore, the destruction rate of cyclic load $\dot{D}_c$ can be expressed as follows:

$$\dot{D}_{\mathrm{c}} = \frac{|\Delta\dot{\bar{u}}|}{\delta_\Sigma}\left[\frac{\bar{T}}{\sigma_{\max}} - C_{\mathrm{f}}\right] H\left(\Delta\bar{u} - \delta_0\right) \quad \text{and} \quad \dot{D}_{\mathrm{c}} \geq 0 \tag{2}$$

with H designating the Heaviside function. $\Delta\bar{u}$ is the resultant separation, and $\Delta\dot{\bar{u}}$ is its increment, which are defined as follows:

$$\begin{cases} \Delta\bar{u} = \sqrt{\Delta u_n^2 + \Delta u_t^2} \\ \Delta\dot{\bar{u}} = \Delta\bar{u}_t - \Delta\bar{u}_{t-\Delta t} \end{cases}$$

$\bar{T}$ is the resultant traction, which can be defined as:

$$\bar{T} = \sqrt{T_n^2 + \frac{T_t^2}{2eq^2}}$$

C_{f} is a parameter to indicate a cyclic load level ratio below which there is no damage initiation. It is the ratio of cohesive zone endurance limit, σ_f to the initial undamaged cohesive normal strength, $C_{\mathrm{f}} = \sigma_f/\sigma_{max,0}$. δ_Σ is accumulated cohesive length, which is used to scale the normalized increment of the effective material separation. It can be considered that when $\Delta_n = \delta_0$, $D = 0$, the material starts to damage; when $\Delta_n = \delta_0 + \delta_\Sigma$, $D = 1$, the area is completely damaged. δ_Σ is generally defined as a multiple of δ_0 in calculations.

Considering that during the loading process, when the resultant separation is greater than the cohesive length, the damage is mainly affected by monotonic loading, so it is necessary to define the failure parameters under monotonic loading:

$$D_m = (\Delta\bar{u}_t - \delta_0)/\delta_\Sigma$$

So there is the following relationship:

$$\dot{D}_m = \frac{\max(\Delta\bar{u}_t) - \max(\Delta\bar{u}_{t-\Delta t})}{\delta_\Sigma} \quad \text{if} \quad \max(\Delta\bar{u}_t) > \delta_0$$

Therefore, if the damage rate of the material under monotonic loading and cyclic loading is considered at the same time, the overall damage parameter of the material can be considered as:

$$D = \int \max(\dot{D}_c, \dot{D}_m)\mathrm{d}t$$

In the cyclic loading process of the element, in addition to the traction and separation relationship of the element during the failure formation process, the behavior of the element during unloading and reloading also needs to be considered. All loading and unloading processes can be considered as being enveloped by the traction-separation curve with failure parameter. All loading and unloading below the envelope curve follow a linear relationship. The slope is equal to the slope of the traction separation curve at zero separated, with damage parameter D considered. The values of current unloading/loading stiffness for normal direction, k_n, is given by:

$$k_n = \frac{\sigma_{\max} e}{\delta_0} = \frac{D\sigma_{\max,0} e}{\delta_0}$$

Therefore, after taking into account the accumulation of damage, the relationship between tension and separation in the process of unloading and reloading is:

$$T_n = T_{n,\max} + k_n(\Delta u_n - \Delta u_{n,\max})$$

During the cyclic loading process, the schematic diagram of the traction-separation curve of the cohesive elements can be shown in Figure 3:

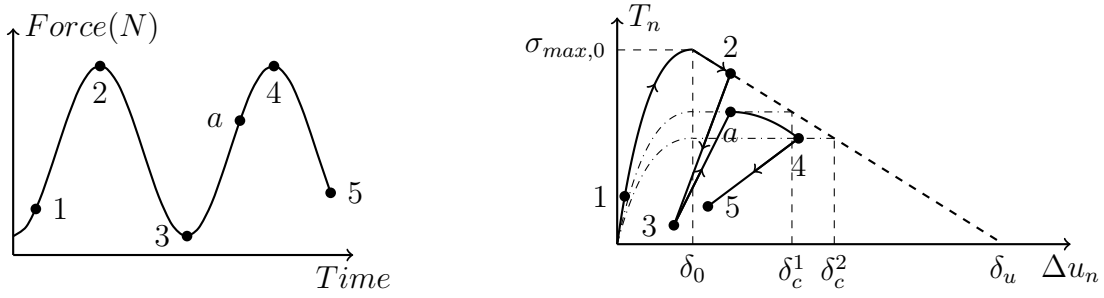

(a) Relationship between external loading and time (b) Traction-separation relationship in cohesive element

Figure 3: The traction-separation relationship in normal cyclic loading

When the external load on the cohesive element is loaded from 1 to 2, (assuming that the separation of the element under load 2 is greater than the cohesive length δ_0), affected by the monotonic damage D_m, the stress of the element first increases to initial cohesive strengths $\sigma_{max,0}$ and then decreases to position 2. When the external load drops from 2 to 3, cohesive element undergoes stress unloading, and the slope of the unloading curve is the stiffness for normal direction $k_n = D\sigma_{max,0}e/\delta_0$. In the process of

cyclic loading, the cyclic loading failure parameter D_c continues to increase. During the loading process of section $3 \rightarrow a$, the stiffness of the element is lower than the stiffness on section 2-3. Due to the combined influence of monotonic and cyclic damage parameters, the maximum stress on the element becomes lower, $\sigma_{max,a} < \sigma_{max,0}$. Assuming that point a reaches the maximum stress, then when the load continues to rise and the failure continues to develop, the maximum stress of the element decreases, and finally reaches the position of point 4, $\sigma_{max,4} < \sigma_{max,a}$. The element unloads along the stiffness, then reaches the position of point 5 at the end.

As the distance between the upper and lower layers of the composite material increases and decreases repeatedly during the cyclic loading process, according to the properties of the beam, the contact of the upper and lower layers needs to be considered to avoid the interference and overlap. A widely used method is to multiply the basic traction-separation curve in equation 1 with a coefficient $\alpha > 1$ so that any value of $\Delta u_n < 0$ is penalized.

$$T_n = \alpha \sigma_{max,0} \left(\frac{\Delta u_n}{\delta_0} \right) \exp \left(1 - \frac{\Delta u_n}{\delta_0} \right) \quad \text{if} \quad \Delta u_n < 0$$

In many studies, the stiffness penalizing factor was taken to be $\alpha = 10$ [15, 28].

3 Model description

The model in this study is based on the benchmark test of Carreras L. et al. [37]. A partially reinforced DCB test with a mid-plane initial defect consisting of a Teflon insert is used, and the dimensions of the partially reinforced DCB specimen is in Figure 4. According to the article, specimens were made of Carbon Fibre Reinforced Polymer (CFRP) plies stacked at 0°. The elastic properties for the unidirectional laminate material is in table 1.

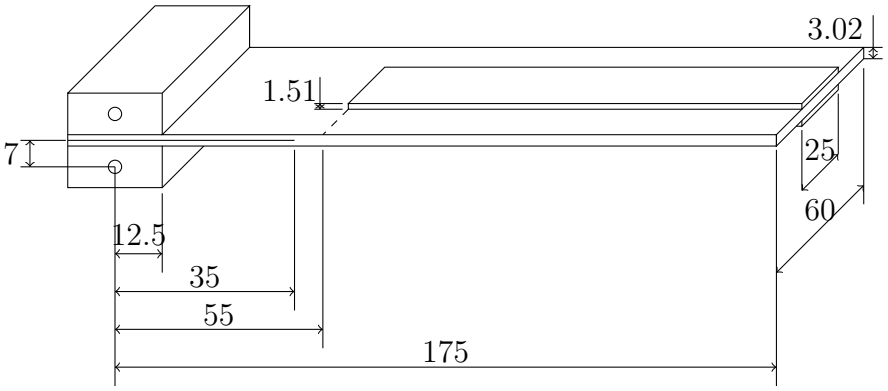

Figure 4: Dimensions of the partially reinforced DCB specimen (units in mm)

The benchmark test includes both quasi-static cases and fatigue loading cases. Quasi-static tests were performed with a constant displacement rate of 1 mm/min on four specimens (A, B, C and D). The fatigue tests consisted of four loading steps (cf. Figure 5):

1. Quasi-static step from the initial unloaded position until 5mm of the prescribed displacement at a loading rate of 1 mm/min;

Table 1: Laminate elastic properties of the validation material

Laminate properties	Values	Units
E_{11}: Longitudinal Young's modulus	154	GPa
$E_{22} = E_{33}$: Transversal Young's modulus	8.5	GPa
$G_{12} = G_{13}$: Shear modulus in longitudinal planes	4.2	GPa
G_{23}: Shear modulus in transversal plane	3.036	GPa
$\mu_{12} = \mu_{13}$: Poisson's ratio in longitudinal planes	0.35	-
μ_{23}: Poisson's ratio in transversal plane	0.4	-

2. Fatigue step with a maximum cyclic displacement of 5 mm and a load ratio of $R = 0.1$;

3. Quasi-static step until 10mm of the prescribed displacement at a loading rate of 1 mm/min;

4. Fatigue step with a maximum cyclic displacement of 10 mmand a load ratio of $R = 0.1$.

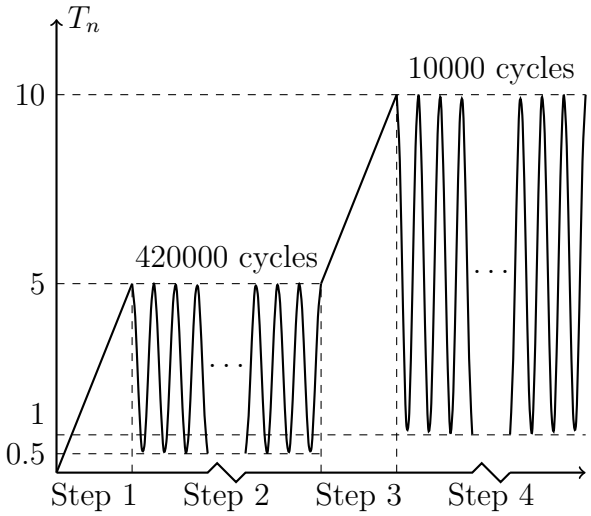

Figure 5: Loading steps of the fatigue tests

In this study, the relevant theory of the cantilever beam was used to derive the load-distance relationship of the partially reinforced DCB under quasi-static conditions and the location of delamination. At the same time, ABAQUS/Standard software was used to perform 3-D FE analysis, and the results of quasi-static and fatigue delamination of the specimen under VCCT and CZM methods were calculated respectively. Figure 6 shows the FE model of specimen. The DCB specimens were meshed using 3-D eight-node brick (C3D8) elements. The VCCT method is implemented by using VCCT to contact bonding conditions and defining keywords; the CZM method is implemented by inserting cohesive elements. A user-defined subroutine (UEL) is also used to define the cohesive fatigue based on the exponential cohesive failure model.

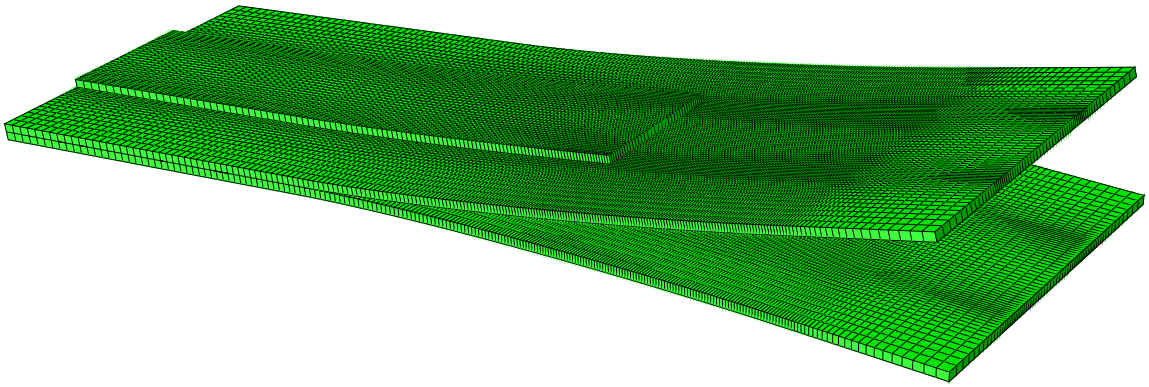

Figure 6: FE model of specimen

4 Analytical model of quasi-static loading

In quasi-static loading, each arm of the test specimen can be simplified into two cantilever beams with different cross-sections. According to the development of damage, energy release rate of the specimen G_I and the delamination length a, the delamination process of the test piece can be divided into four stages:

1. $a = a_0$, $G_I \leq G_{Ic}$, the delamination area has not developed;
2. $a_0 < a < a_1$, $G_I = G_{Ic}$, delamination begins to develop in areas without reinforcement;
3. $a \to +a_1$, $G_I \leq G_{Ic}$, delamination stops at the connection area of common region and reinforce region, and strain energy continues to accumulate as the traction force increases;
4. $a > a_1$, $G_I = G_{Ic}$, delamination develops in the reinforce area.

The potential energy of the reinforce DCB specimen, U_p, is given by:

$$U_p = U_s - Pu$$

where U_s is the strain energy of the specimen, P is the loading force in vertical direction on the upper arm of the specimen, and u is the corresponding opening distance. The strain energy of a bending beam can be calculated by:

$$U_s = \int_0^l \frac{M^2}{2E'I} dx$$

with length l, applied moment M, elastic modulus E' and the second moment of inertia I of the beam.

4.1 Delamination develops in region without reinforcement

The specimen can be divided into three free bodies, which are shown in Figure 7. The strain energy of the whole specimen can be expressed as:

$$U_s = \int_0^a \frac{(Px)^2}{2E'I_1} dx + \int_0^a \frac{(Px)^2}{2E'I_2} dx$$

I_i is the second moment of inertia in part i of the specimen, $I_1 = I_2 = w_1 h_1^3/12 = I$. Since the displacement of the fixed arm is 0, according to the Castigliano's second theorem, the moving distance of the loading arm can be given by:

$$u = \frac{\partial U_s}{\partial P} = \frac{2Pa^3}{3E'I}$$

Assuming that the end face of the delamination front is straight, then under this loading condition, the energy release rate G_I can be calculated as:

$$G_I = -\frac{1}{w}\frac{\partial U_p}{\partial a} = \frac{P^2 a^2}{E'Iw}$$

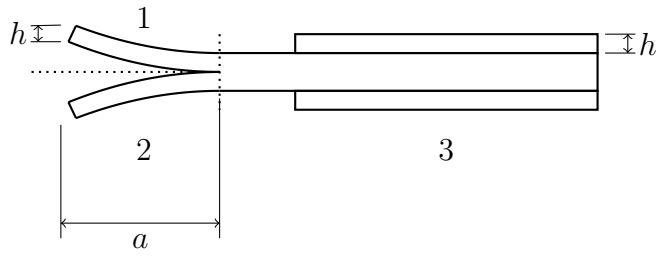

Figure 7: Three free bodies the specimen can be divided into

At the beginning of the loading stage, $a = a_0$, $G_I \leq G_{Ic}$, the loading force will increase linearly with the increase of the separation distance, until $G_I = G_{Ic}$, where the loading force reaches the maximum value. At this stage, loading and separation satisfy the following relationship:

$$P = \frac{3E'I}{2a_0^3}u \tag{3}$$

When $a_0 < a < a_1$, $G_I = G_{Ic}$, delamination begins to develop in areas without reinforcement. According to the relationship between energy release rate, loading and displacement, the following equations can be derived:

$$u = \sqrt{\frac{4wa^4 G_{Ic}}{9E'I}}, \quad P = \sqrt{\frac{2}{3u}}(wG_{Ic})^{0.75}(E'I)^{0.25} \tag{4}$$

4.2 Delamination develops in region with reinforcement

When a is close to or greater than a_1, due to the change of the cross-sectional shape, the strain energy calculation formula of the specimen will also change accordingly. Similar to the Section 4.1 , the specimen can be divided into five free bodies, which are shown in Figure 8. The strain energy of the whole specimen is:

$$U_s = \int_0^{a_1} \frac{(Px)^2}{2E'I_1}dx + \int_0^{a_1} \frac{(Px)^2}{2E'I_2}dx + \int_{a_1}^{a} \frac{(Px)^2}{2E'I_3}dx + \int_{a_1}^{a} \frac{(Px)^2}{2E'I_4}dx \quad \text{if} \quad a \geq a_1$$

Assume that the cross-section of third and fourth part are shown in Figure 9, the centroid coordinates and the second moment of inertia in these two parts can be calculated as:

$$y_c = \frac{w_2 h_2^2 - w_1 h_1^2}{2(w_1 h_1 + w_2 h_2)}, \quad z_c = 0, \quad I_{y_c} = \frac{w_1 h_1^3}{12} + w_1 h_1 \left(\frac{h_1}{2} + y_c\right)^2 + \frac{w_2 h_2^3}{12} + w_2 h_2 \left(\frac{h_2}{2} - y_c\right)^2$$

and $I_3 = I_4 = I_{y_c}$. Therefore, the calculation equations for separation displacement and energy release rate are:

$$u = \frac{\partial U_s}{\partial P} = \frac{2Pa_1^3}{3E'I} + \frac{2P(a^3 - a_1^3)}{3E'I_{y_c}}$$
$$G_I = -\frac{1}{w}\frac{\partial U_p}{\partial a} = \frac{P^2a^2}{E'I_{y_c}w}$$

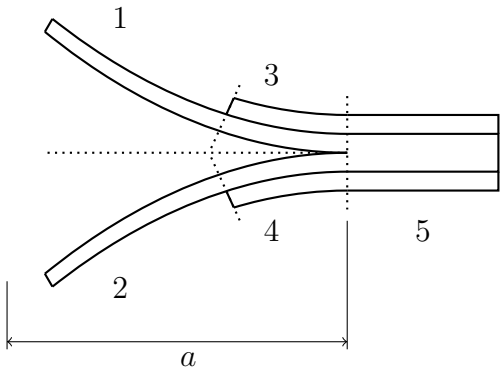

Figure 8: Five free bodies the specimen can be divided into

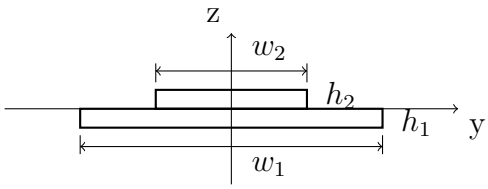

Figure 9: Cross-section of the specimen arm with reinforcement

When the delamination stops at the connection area of common region and reinforce region, and strain energy continues to accumulate as the traction force increases, $a \to +a_1$, $G_I \leq G_{Ic}$, loading and separation relationship can be expressed by the following equation:

$$P = \frac{3E'I}{2a_1^3}u \tag{5}$$

When delamination develops in the reinforce area, $a > a_1$, $G_I = G_{Ic}$,

$$\begin{aligned} u &= \frac{2\sqrt{G_{Ic}E'I_{y_c}w_1}}{3a} \times \left(\frac{a_1^3}{E'I} + \frac{a^3 - a_1^3}{E'I_{y_c}}\right) \\ P &= \sqrt{G_{Ic}E'I_{y_c}w_1}/a \end{aligned} \tag{6}$$

4.3 Damage development analysis

According to the analysis results in Section 4.1 and 4.2 , the development of delamination damage can be divided into 4 stages, and the values of a and u can be used to judge the stage of delamination.

At different stages, the relationship between loading force and separation distance is:

$$\text{stage 1:} \begin{cases} P = \dfrac{3E'I}{2a_0^3}u \\ u \le u_1 \end{cases} \qquad \text{stage 2:} \begin{cases} P = \sqrt{\dfrac{2}{3u}}(wG_{Ic})^{0.75}(E'I)^{0.25} \\ u_1 \le u < u_2 \end{cases}$$

$$\text{stage 3:} \begin{cases} P = \dfrac{3E'I}{2a_1^3}u \\ u_2 \le u < u_3 \\ a \to a_1 \end{cases} \qquad \text{stage 4:} \begin{cases} u = \dfrac{2\sqrt{G_{Ic}E'I_{y_c}w_1}}{3a} \times \left(\dfrac{a_1^3}{E'I} + \dfrac{a^3 - a_1^3}{E'I_{y_c}}\right) \\ P = \sqrt{G_{Ic}E'I_{y_c}w_1}/a \\ a > a_1 \end{cases}$$

The values of $u1$, $u2$, and $u3$ can be calculated by the following equation:

$$u_1 = \frac{2a_0^2}{3}\sqrt{\frac{wG_{Ic}}{E'I}}, \quad u_2 = \frac{2a_1^2}{3}\sqrt{\frac{wG_{Ic}}{E'I}}, \quad u_3 = \frac{2a_1^2}{3}\sqrt{\frac{wG_{Ic}}{E'I_{y_c}}}$$

According to the above equations, the separation-loading curve during the delamination process of the specimen is in Figure 10. In the model analysis of the third and fourth stages, the assumption that the damage front is a straight line is still adopted. However in these two stages, due to the influence of the strengthening structure, the shape of the failure front edge will be curved. In the initial part of the third stage, as the separation distance increases, delamination failure will occur in advance in the area away from the reinforcement. The width of delamination leading edge $w > w_1$, and increases with the increase of the separation. The loading force required to preform the separation would be lower than the model with straight front. Therefore, it is necessary to consider an coefficient that increases with u in the third stage, and to be multiply with the loading force P. The figure also indicated that at the beginning of the fourth stage, the specimen exhibits unstable delamination propagation. Combining the above two reasons, the curve of delamination development is shown in dashed lines.

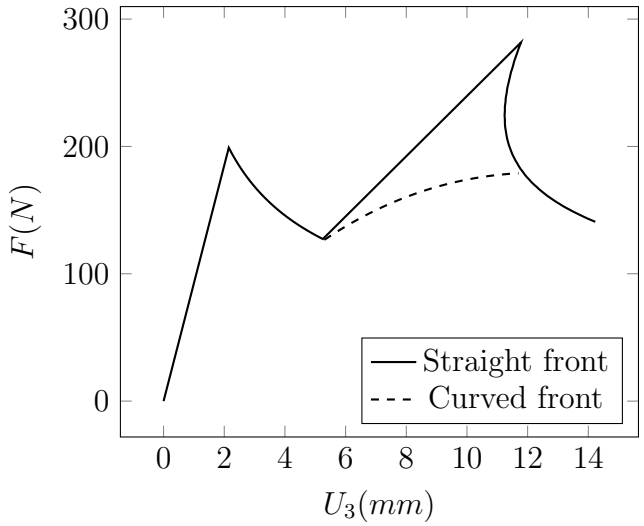

Figure 10: Load-displacement curves based on analytical model

5 Results and discussion

5.1 Quasi-static loading

The results of the analysis, the experiment, and the simulation of both VCCT and cohesive elements are shown in Figure 11. The results show that the load-displacement cruves obtained by the four methods can obviously be divided into four parts, corresponding to the four stages of delamination development. The simulation results of the VCCT and cohesive elements are close to the experiment results, especially in the first and third stages. In the second and fourth stages, the results of VCCT and cohesive simulation have a certain lag compared to the experiment. According to the literature[40], this is related to the damping defined in simulation process in order to avoid non-linearity, which may cause simulation to diverge. In the fourth stage, under the influence of both the increase of the delamination distance a and the increase of the geometric stiffness of the specimen's arm, the delamination develops faster, thus the lagging of the curve is more obvious.

The curve of the analytical model shows greater rigidity. This is due to the delamination area has been treated as a simple cantilever beam during the whole analysis process, and the influence of the uneven front edge of the delamination on the result is ignored. Since in both experiment and simulation, the stiffness and energy release rate are lower than the analytical model, the loading force at each stage are also smaller than the analytical model.

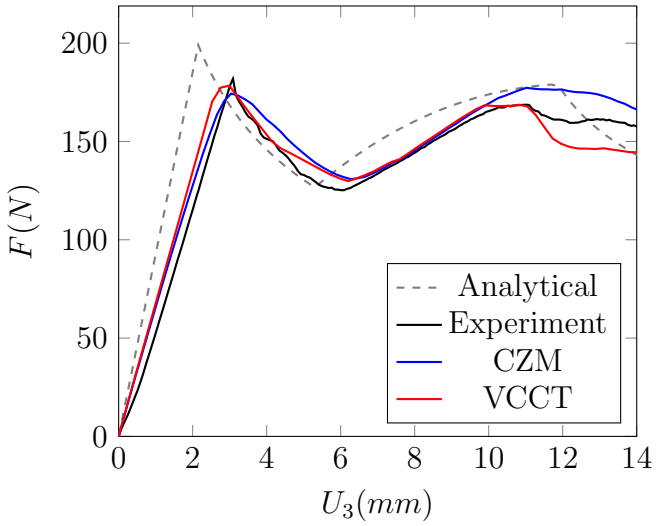

Figure 11: Load-displacement under quasi-static loading

Figure 12 shows the delamination front positions of analysis, experiment, and the VCCT/cohesive elements simulations under quasi-static loading. No significant differences were found between the experimental results and the simulation, and the delamination length of the analysis model is close to the other three results, but due to the assumption that damage front is straight, the shape of the damage front in analysis model is different from the experiments and simulations.

By comparing the simulated delamination front position with the experiment, it can be found that the delamination of the simulation and the test results are pretty similar before the damage front enters the

partially reinforced region. But after the crack front develops close to the reinforced region, the damage at both ends of the crack front will continue to advance around the region, while the middle section moves much slower. However, when the delamination front move gradually forward, until it completely invades the reinforced region, the unsteady damage development discussed in Section 4.3 occurs: delamination front of the reinforced area advances suddenly, from lagging behind the non-reinforced area to rapidly developing ahead of the unreinforced area.

The shapes of the damage front of the cohesive elements in the reinforced region are very similar to the experimental results at most part, but slightly lags behind the in the later stage, resulting in a larger overall stiffness of the test piece. Therefore, at the end of Figure 11, the loading force at cohesive elements model is greater than that of the test. The VCCT method keeps the failure front straight in the area with the reinforcement, which is related to the characteristic of the VCCT model that energy release rate is calculated based on the local thickness. This characteristic of VCCT results in the shape distortion of the failure front edge in the reinforced region, therefore the contact surface is released prematurely, which causes the failure front edge to be more advanced than the other results, and the structural rigidity of the specimen decreases. Therefore, at the end of Figure 11, The delamination loading force of VCCT model is less than the test results.

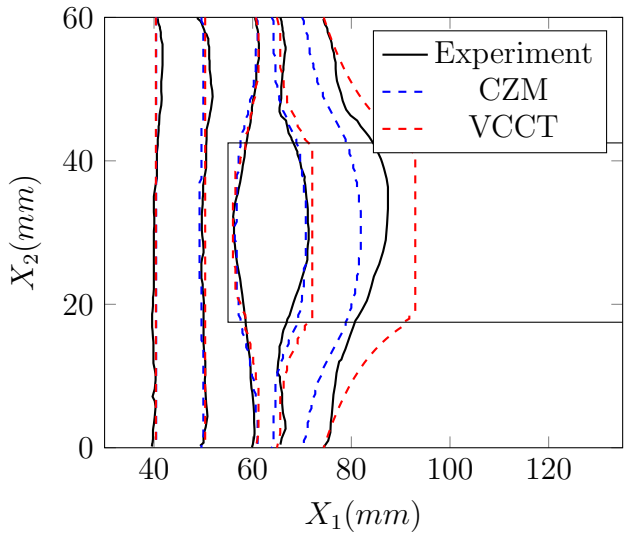

Figure 12: Delamination front position in quasi-static loading

5.2 fatigue loading

The load-displacement relationship of the experiment and VCCT/CZM simulation are presented in Figure 13. It is apparent from this figure that the cohesive element model are relatively close to the experiment, and correspond to the experimental displacement-load curves in all four loading steps. while the calculation results of the VCCT model can correspond in the first and second loading steps, but a significant difference is shown in the third analysis step between the VCCT model and the experimental or cohesive elements results. The reason is that in second loading step, the VCCT model uses the low-cycle fatigue

failure criterion which based on Paris's law to calculate the separation conditions of the nodes at damage front; at the end of a loading with 45,000 cycles, some micro-damages have occurred in the material at the failure front edge. and they will be the foundation of further dameges. However in the third step of loading, the VCCT model switches to the standard VCCT criterion to determine the separation conditions of the nodes, and the micro-damage caused by fatigue has no effect on this loading step. Therefore the continued delamination of the VCCT model is consistent with the trend in Figure 11, which is greater than the experimental data or the cohesive elements results. The fourth loading step continues to calculate the fatigue failure based on the results of the third loading step, but let aside the micro-damage caused at this step. Affected by the third loading step, its load value is also greater than the test data and the calculation result of the cohesive element.

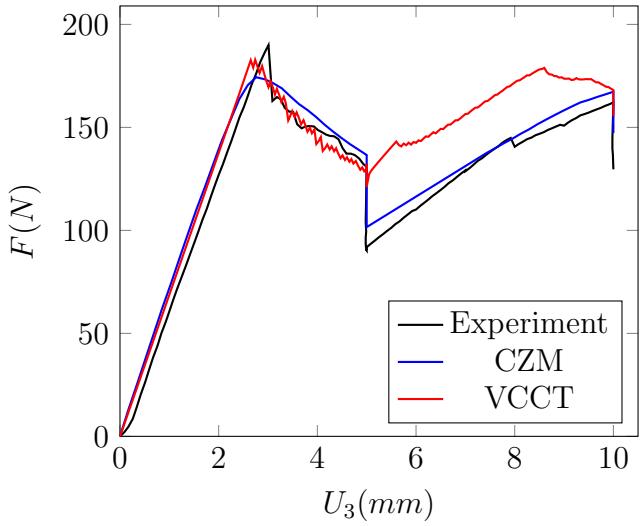

Figure 13: Load-displacement under fatigue loading

The delamination front positions of experiment and simulation of VCCT/CZM models under fatigue loading can be compared in Figures 14 and 15. In all loading steps, the delamination front positions of the experiment and CZM simulation model are similar. However, The analysis in Figure 13 indicates that the damage of VCCT in load step 2 does not inherit the micro-damage in load step 1, which results in the slower development in VCCT delamination in Figure 14, as the nodes at the crack front behaves stronger without pre-damage. Similar to the development of delamination under quasi-static loading, the delamination front develops extremely slowly near the reinforced region, while the crack front moves faster at the other area. In the third loading step, the VCCT method is again converted from the fatigue failure criterion to the VCCT criterion, and the separation of the nodes is continued to be calculated based solely on the opening at this time. Therefore, the position of the delamination front is close to that of the specimen in Figure 12 which has not undergone fatigue loading and have the same opening. In the fourth loading step, the VCCT method switches back to the fatigue failure criterion one more time, and the micro-damage caused by monotonic loading does not have its due effect on this loading step. The VCCT model loses the information of micro-damdage every time the failure criterion changed, thus after several repeated changes, the position of the crack front in VCCT model has significantly deviated from

the results of the experiment and CZM model.

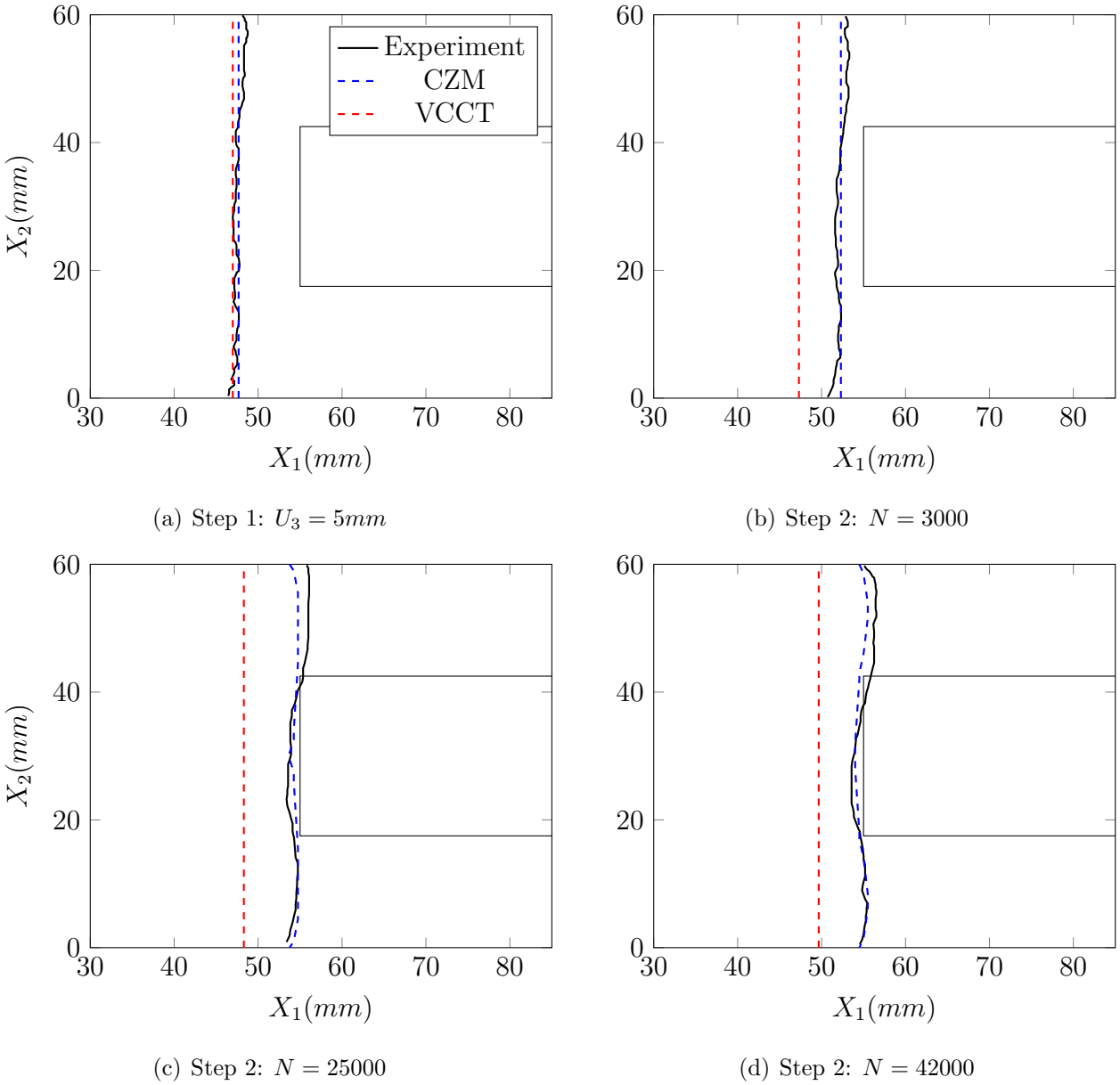

(a) Step 1: $U_3 = 5mm$

(b) Step 2: $N = 3000$

(c) Step 2: $N = 25000$

(d) Step 2: $N = 42000$

Figure 14: Delamination front position during steps 1 and 2

Combining the results of the analysis model, test data, and two different simulation methods (VCCT and CZM), it can be concluded that there is still a big difference between the partially reinforced DCB and the normal DCB. Compared with normal DCB, the maximum load that the reinforced DCB can carry will not be higher, but it can have multiple load peaks, which avoids the rapid decrease in the overall stiffness of the specimen once the first peak is passed during monotonic or cyclic loading, and results in rapid failure. However, the partially reinforced DCB will be unstable when the delamination damage front edge completely enters the reinforced part, causing the damage front to advance a certain distance quickly. This feature is unique in partially reinforced DCB.

Comparing the simulation results of VCCT method and CZM on delamination, it can be found that

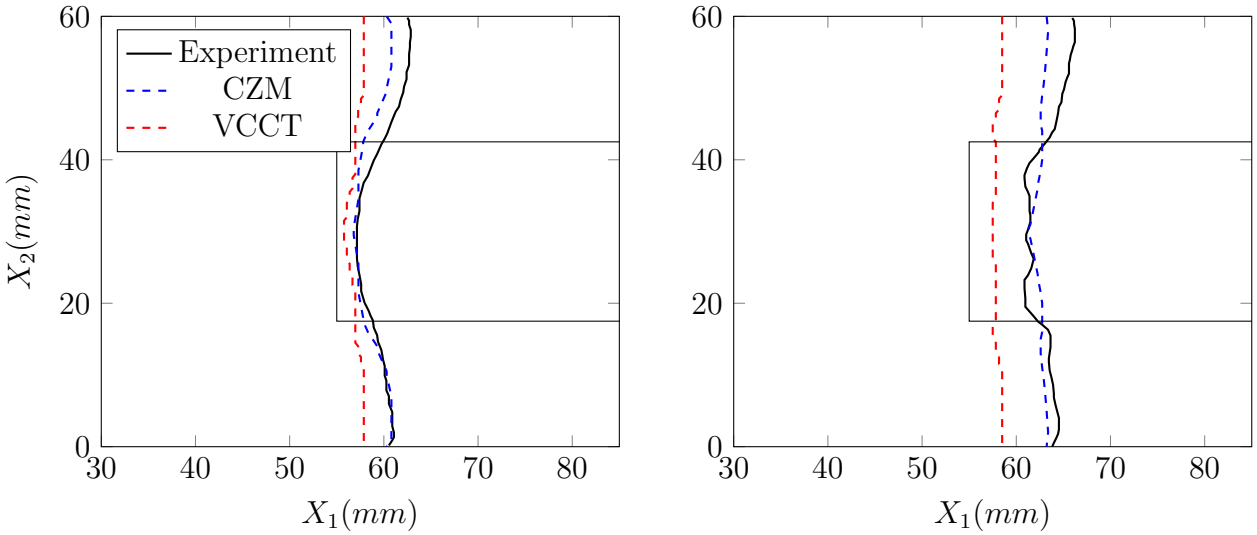

(a) Step 3: $U_3 = 10mm$

(b) Step 4: $N = 1500$

(c) Step 4: $N = 3000$

(d) Step 4: $N = 10000$

Figure 15: Delamination front position during steps 3 and 4

when VCCT method simulates partially reinforced DCB, the shape of the delamination front in reinforced area is distorted, which causes the load in the load-displacement curve to be smaller than the true value. When using the VCCT method to simulate the delamination of partially reinforced DCB under the repeated action of monotonic and cyclic load, VCCT will discard the micro-damage data calculated in the previous step every time the failure criterion is switched, thus larger errors develops with the increase in number of switching times of the destruction criterion. However, the CZM uses both the monotonic damage D_m and the cyclic damage D_c to indicate the degree of damage of the cohesive elements. Under different load steps, the damage parameters can be transmitted from the previous one to the next, so there is no information loss of micro-damage, and makes it a relatively reliable method in simulating partially reinforced DCB.

6 Conclusion

In order to analyze the quasi-static and fatigue delamination process of composite laminates with uneven thickness and its simulation methods, in this research, the delamination process of a partially reinforced DCB was studied using theory and VCCT and CZM simulation methods, then the experimental results were used as benchmark to make the comparison. The results show that the delamination in areas without reinforcement behaves the same as that of standard DCB, that loading increases with the increase of separation distance, then decreases with the increase of delamination distance. However, when the delamination front is close to the partially reinforced composite laminate area, the shape of the crack front will bend around the reinforcement, decreasing the energy release rate of the specimen, increasing the load or fatigue cycle required for delamination, and generating a second peak. When the delamination front completely enters the reinforced area, the specimen will develop a sudden unstably delamination, whick causes the delamination front under the reinforced area moves forward rapidly. This is caused by the sudden release of strain energy. This process can be observed not only in theory and experiment, but also in VCCT and CZM simulations.

By comparing the VCCT method and CZM in simulating the delamination process of the partially reinforced DCB specimen, it can be found that the results of the load-displacement relationship of both methods are similar to the test in quasi-static delamination. However, the crack front of VCCT will remain straight after it enters the area of local reinforcement, which is inconsistent with the test results; on the contrary, the delamination front edge of the CZM is more consistent with the test results. When the finite element method is used to simulate the delamination that alternately switching between quasi-static and fatigue, the VCCT method cannot match the test results due to its own characteristics. This is because VCCT uses different failure criteria under steady-state and fatigue load steps, thus the effects of micro damage cannot be transferred between different load steps, which makes VCCT method not suitable for simulating the fatigue delamination process of composite laminates with uneven thickness. At the same time, in the simulation using Roe's exponential CZM model, because the damage parameter under monotonic load D_m and the damage parameter under cyclic load D_c affect the tension-separation relationship of the element at the same time, and the damage is transmitted between loading steps, the CZM simulation result is much more similar to the test results.

In future work, it is necessary to further study the parameters of the CZM, so that it can simulate the load-displacement relationship and the position of the delamination front in the later stage of rapid delamination in the strengthened area more accurately.

References

[1] Md Sarower Tareq, Bodiuzzaman Jony, Shaik Zainuddin, Mohammad Al Ahsan, and Mahesh V Hosur. Fatigue analysis and fracture toughness of graphene reinforced carbon fibre polymer composites. *Fatigue Fract Eng Mater Struct*, 44(2):461–474, 2021.

[2] Sabrina Vantadori, Andrea Carpinteri, Karolina Głowacka, Fabrizio Greco, Tomasz Osiecki, Camilla Ronchei, and Andrea Zanichelli. Fracture toughness characterisation of a glass fibre-reinforced plastic composite. *Fatigue Fract Eng Mater Struct*, 44(1):3–13, 2021.

[3] Hyunbum Park and Changduk Kong. Experimental study on barely visible impact damage and visible impact damage for repair of small aircraft composite structure. *Aerosp Sci Technol*, 29(1):363–372, 2013.

[4] Rosa De Finis, Davide Palumbo, and Umberto Galietti. Evaluation of damage in composites by using thermoelastic stress analysis: A promising technique to assess the stiffness degradation. *Fatigue Fract Eng Mater Struct*, 43(9):2085–2100, 2020.

[5] Alan Arnold Griffith. Vi. the phenomena of rupture and flow in solids. *Philos T R Soc Lond*, 221(582-593):163–198, 1921.

[6] George R Irwin and JA Kies. Critical energy rate analysis of fracture strength. *Spie Milestone series MS*, 137:136–141, 1997.

[7] Donald S Dugdale. Yielding of steel sheets containing slits. *J Mech Phys Solids*, 8(2):100–104, 1960.

[8] Grigory I Barenblatt. The formation of equilibrium cracks during brittle fracture. general ideas and hypotheses. axially-symmetric cracks. *J Appl Math Mech*, 23(3):622–636, 1959.

[9] Paul C Paris. A rational analytic theory of fatigue. *Trends Engin*, 13:9, 1961.

[10] Paolo S Valvo. A revised virtual crack closure technique for physically consistent fracture mode partitioning. *Int J Fracture*, 173(1):1–20, 2012.

[11] Albert Turon Travesa, Josep Costa i Balanzat, Pedro Manuel Ponces Rodrigues de Castro Camanho, and Carlos G Dávila. Simulation of delamination propagation in composites under high-cycle fatigue by means of cohesive-zone models. © *NASA TP Technical Reports, 2006, núm. 214532*, 2006.

[12] DC Noorman. Cohesive zone modelling in adhesively bonded joints: Analysis on crack propagation in adhesives and adherends. 2014.

[13] Bent F Sørensen and Torben K Jacobsen. Determination of cohesive laws by the j integral approach. *Eng Fract Mech*, 70(14):1841–1858, 2003.

[14] Benoît Blaysat, Johan PM Hoefnagels, Gilles Lubineau, Marco Alfano, and Marc GD Geers. Interface debonding characterization by image correlation integrated with double cantilever beam kinematics. *Int J Solids Struct*, 55:79–91, 2015.

[15] KL Roe and Th Siegmund. An irreversible cohesive zone model for interface fatigue crack growth simulation. *Eng Fract Mech*, 70(2):209–232, 2003.

[16] Anonymus AC09036782. *Standard test method for mode I interlaminar fracture toughness of unidirectional fiber-reinforced polymer matrix composites*. ASTM Internat., 2007.

[17] Iurii Burda, Michel Barbezat, and Andreas J Brunner. Delamination resistance of gfrp-epoxy rods with nanoparticle-and microparticle-modified matrix and its correlation with the fracture properties of epoxy nanocomposites. *Fatigue Fract Eng Mater Struct*, 43(2):292–307, 2020.

[18] S Mall and W Steven Johnson. Characterization of mode i and mixed-mode failure of adhesive bonds between composite adherends. In *Composite materials: testing and design (seventh conference)*. ASTM International, 1986.

[19] Spandan Maiti and Philippe H Geubelle. A cohesive model for fatigue failure of polymers. *Eng Fract Mech*, 72(5):691–708, 2005.

[20] X-P Xu and A Needleman. Void nucleation by inclusion debonding in a crystal matrix. *Model Simul Mater Sc*, 1(2):111, 1993.

[21] Albert Turon, Carlos G Davila, Pedro Ponces Camanho, and Josep Costa. An engineering solution for mesh size effects in the simulation of delamination using cohesive zone models. *Eng Fract Mech*, 74(10):1665–1682, 2007.

[22] Ofir Shor and Reza Vaziri. Application of the local cohesive zone method to numerical simulation of composite structures under impact loading. *Int J Impact Eng*, 104:127–149, 2017.

[23] Alireza Rafie, Hamidreza Madadi, Amin Farrokhabadi, and Miguel Herráez. In situ strength analysis of cross-ply composite laminates containing defects and interleaved woven layer using a computational micromechanics approach. *Fatigue Fract Eng Mater Struct*, 44(5):1225–1240, 2021.

[24] Hamidreza Madadi, Mohsen Naghdinasab, and Amin Farrokhabadi. Numerical investigation of matrix cracking propagation in cross-ply laminated composites subjected to three-point bending load using concurrent multiscale model. *Fatigue Fract Eng Mater Struct*, 43(6):1159–1169, 2020.

[25] Francis MG Ramírez, Marcelo FSF de Moura, Raul DF Moreira, and Filipe GA Silva. A review on the environmental degradation effects on fatigue behaviour of adhesively bonded joints. *Fatigue Fract Eng Mater Struct*, 43(7):1307–1326, 2020.

[26] G Giuliese, A Pirondi, and F Moroni. A cohesive zone model for three-dimensional fatigue debonding/delamination. *Proc Mat Sci*, 3:1473–1478, 2014.

[27] JL Fan and XL Guo. Numerical simulation on elastic-plastic fatigue crack growth behavior. *J Mech Eng Sci*, 51(10):33–40, 2015.

[28] Susana del Busto, Covadonga Betegón, and Emilio Martínez-Pañeda. A cohesive zone framework for environmentally assisted fatigue. *Eng Fract Mech*, 185:210–226, 2017.

[29] Siroos Ahmadi and Afshin Zeinedini. Experimental, theoretical and numerical investigation of the drilling effects on mode i delamination of laminated composites. *Aerosp Sci Technol*, 104:105992, 2020.

[30] S Karmakov, F Cepero-Mejías, and JL Curiel-Sosa. Numerical analysis of the delamination in cfrp laminates: Vcct and xfem assessment. *Compos Part C-Open A*, 2:100014, 2020.

[31] Hossein Hosseini-Toudeshky, Mir Ali Ghaffari, and Bijan Mohammadi. Mixed-mode crack propagation of stiffened curved panels repaired by composite patch under combined tension and shear cyclic loading. *Aerosp Sci Technol*, 28(1):344–363, 2013.

[32] A Pirondi, G Giuliese, F Moroni, ANDREA Bernasconi, and AZHAR Jamil. Comparative study of cohesive zone and virtual crack closure techniques for three-dimensional fatigue debonding. *J Adhes*, 90(5-6):457–481, 2014.

[33] Mohammad Heidari-Rarani and Mousa Sayedain. Finite element modeling strategies for 2d and 3d delamination propagation in composite dcb specimens using vcct, czm and xfem approaches. *Theor Appl Fract Mech*, 103:102246, 2019.

[34] Aniello Riccio, A Raimondo, G Di Felice, and F Scaramuzzino. A numerical procedure for the simulation of skin–stringer debonding growth in stiffened composite panels. *Aerosp Sci Technol*, 39:307–314, 2014.

[35] Waqas Anwar, M Zubair Khan, Asif Israr, Shahid Mehmood, and Nazeer A Anjum. Effect of structural dynamic characteristics on fatigue and damage tolerance of aerospace grade composite materials. *Aerosp Sci Technol*, 64:39–51, 2017.

[36] A Delbariani-Nejad, M Malakouti, and A Farrokhabadi. Reliability analysis of metal-composite adhesive joints under debonding modes i, ii, and i/ii using the results of experimental and fem analyses. *Fatigue Fract Eng Mater Struct*, 42(12):2644–2662, 2019.

[37] Laura Carreras, Jordi Renart, Albert Turon, Josep Costa, Brian Lau Verndal Bak, Esben Lindgaard, F Martin de la Escalera, and Yasser Essa. A benchmark test for validating 3d simulation methods for delamination growth under quasi-static and fatigue loading. *Compos Struct*, 210:932–941, 2019.

[38] KN Shivakumar, PW Tan, and JC Newman Jr. A virtual crack-closure technique for calculating stress intensity factors for cracked three dimensional bodies. 1988.

[39] A Needleman. An analysis of decohesion along an imperfect interface. In *Non-Linear Fracture*, pages 21–40. Springer, 1990.

[40] Ronald Krueger. An approach to assess delamination propagation simulation capabilities in commercial finite element codes. 2008.